Title: Adaptively introgressed Neandertal haplotype at the OAS locus functionally impacts innate immune responses in humans.

Authors

Aaron J. Sams[1,* †] (as2847@cornell.edu)

Anne Dumaine[2†] (dumaine.anne@gmail.com)

Yohann Nédélec[2,3†] (yohann.nedelec@gmail.com)

Vania Yotova[2] (vania.g.yotova@gmail.com)

Carolina Alfieri[2,4] (carolina.alfieri@recherche-ste-justine.qc.ca)

Jerome E. Tanner[2] (jetanner@videotron.ca)

Philipp W. Messer[1,*‡] (messer@cornell.edu)

Luis B. Barreiro[2,5,* ‡] (luis.barreiro@umontreal.ca)

Affiliations

[1]Department of Biological Statistics and Computational Biology, Cornell University, Ithaca, NY

[2]Department of Genetics, Sainte-Justine Hospital Research Centre, University of Montreal, Montreal, Qc, Canada

[3]Department of Biochemistry, University of Montreal, Montreal, Qc, Canada

[4]Department of Microbiology and Immunology, University of Montreal, Montreal, Qc, Canada

[5]Department of Pediatrics, University of Montreal, Montreal, Qc, Canada

[†]These authors contributed equally to this work

[‡]These authors jointly supervised this work

[*]Corresponding author

Abstract

The 2'-5' oligoadenylate synthetase (OAS) locus encodes for three OAS enzymes (OAS1-3) involved in innate immune response. This region harbors high amounts of Neandertal ancestry in non-African populations; yet, strong evidence of positive selection in the OAS region is still lacking. Here we used a broad array of selection tests in concert with neutral coalescent simulations to firmly demonstrate a signal of adaptive introgression at the OAS locus. Furthermore, we characterized the functional consequences of the Neandertal haplotype in the transcriptional regulation of OAS genes at baseline and infected conditions. We found that cells from people with the Neandertal-like haplotype express lower levels of *OAS3* upon infection, as well as distinct isoforms of *OAS1* and *OAS2*. Notably, the Neandertal-introgressed haplotype reintroduced an ancestral splice variant of *OAS1* encoding a more active protein, suggesting that adaptive introgression occurred as a means to resurrect adaptive variation that had been lost outside Africa.

Keywords: Natural selection, introgression, innate immunity

Background

Whole genome sequencing of several archaic human genomes [1-5] representing Neandertals and an as yet geographically and paleontologically unknown population referred to as Denisovans has revealed gene flow between these populations and the ancestors of present-day humans. Neandertal ancestry makes up approximately 0.5-2 percent of the ancestry of most living humans, with higher

amounts of Neandertal ancestry found outside of Africa [6-8]. While it seems that there may have been widespread purifying selection against Neandertal ancestry in humans [6,8,9], some positive selection on Neandertal genes (adaptive introgression) has also been observed [10,11]. Neandertals and other archaic populations inhabited Eurasia for several hundred thousand years [12] and were likely well adapted to their environments. Therefore, some genetic variation inherited from these archaic humans may have been adaptive in modern humans, particularly across phenotypes that are strongly influenced by direct interactions with the surrounding environment [10], such as our immune response to infectious agents [13].

The OAS locus on chromosome 12, which harbors three genes (*OAS1, OAS2, OAS3*) encoding the 2'-5' oligoadenylate synthetase enzymes has received considerable attention due to its clear signatures of multiple archaic haplotypes in populations outside of Africa [14,15], and the critical role of OAS genes in the innate immune response to viruses [16]. Mendez and colleagues [17] first identified an introgressed haplotype of *OAS1* from Denisovans that is restricted to individuals in Indonesia and Melanesia. Later, these authors [15] identified a Neandertal haplotype at the OAS locus that spans a ~190 kilobase region between two surrounding recombination hotspots.

The elevated frequency of the Neandertal derived alleles in the OAS locus (Figure 1) relative to average levels of Neandertal ancestry in Europeans [6] , along with the key role OAS genes play in protective immunity against viral infections raises

70 the possibility that introgressed Neandertal haplotypes at OAS may have been
71 adaptive in modern humans. While some studies provide suggestive evidence of
72 adaptive introgression at the OAS locus [6,11], strong evidence of positive
73 selection in the OAS region is still lacking. Indeed, several studies failed to reject
74 a model of neutral evolution for the Neandertal haplotype when using standard
75 neutrality tests [15,18].

76 We hypothesize that the overall lack of signals of selection in the OAS region
77 stems from the low power of standard neutrality tests to detect adaptive
78 introgression [19]. Here we circumvent this issue by testing the hypothesis of
79 adaptive introgression using extensive neutral coalescent simulations specifically
80 tailored to match the genomic features of the OAS region in combination with
81 several empirical observations of Eurasian genetic variation, and ancient DNA
82 data from Eurasia. We firmly demonstrate a population genetic signal of adaptive
83 introgression at the OAS locus and characterize the functional consequences of the
84 Neandertal haplotype in the transcriptional regulation of OAS genes in
85 macrophages and peripheral blood mononuclear cells (PBMCs) at baseline and
86 infected conditions. We note that the term 'adaptive introgression' will be used in
87 a broad sense, as our tests do not allow us to determine the exact timing when
88 selection started to act on the Neanderthal alleles.

89 **Results**

90 Mendez *et al*. [15] previously reported evidence of archaic introgression at the
91 OAS locus. We first verified these results, using data from phase 3 of the 1000

92 Genomes Project [20], by examining the relationships of all modern human
93 sequences at the OAS locus with the Altai Neandertal, Denisovan, and an inferred
94 ancestral sequence. Clustering the human haplotypes resulted in 10 consensus
95 sequences representing human haplotype clusters, which we combined with the
96 archaic sequences in a neighbor-joining tree (Methods, Figure 1A, S1). This tree
97 confirms that the Denisovan haplotype is not present in the population samples
98 represented in the 1000 Genomes Project dataset. In contrast, the Neandertal
99 haplotype is found at relatively high frequencies outside of Africa, reaching
100 highest frequencies in European population samples (up to 43%, Figure 1B).
101 Additionally, we corroborate the finding of Mendez and colleagues [15] that
102 Neandertal-like haplotypes in the OAS region are too long to have resulted from
103 incomplete lineage sorting (ILS) ($P \leq 2x10^{-3}$, Methods).

104 To investigate the hypothesis of non-neutral evolution at the OAS locus we first
105 tested whether the observed frequencies of Neandertal-like sites (NLS) in the OAS
106 region are higher than expected under neutrality. We defined NLS as bi-allelic
107 SNPs with derived alleles that are shared between Neandertals and a non-African
108 population sample, but absent in a sub-Saharan African sample [6,21,22].
109 Specifically, we simulated the expected allele frequency of NLS under neutrality,
110 using a demographic model based on previously inferred parameters of human
111 demographic history [23-25](Figure S1, Table S1). We considered both a model
112 with a single pulse of Neandertal introgression occurring over a span of 500 years
113 into the ancestral Eurasian population after their population split from Africa, and
114 two additional two-pulse models (Figure S1, Table S1). We found that in all

115 European populations (with the exception of Finnish (FIN)), the highest frequency
116 NLS fall in the extreme 1% of all simulations and are significantly elevated in
117 frequency (all five European samples pass FDR < 0.05, see Table S2), regardless
118 of whether we assume a single-pulse introgression model (Figure 2A) or two-pulse
119 introgression models (Figure S3), indicating that the high frequencies of NLS
120 found in most European populations likely reflects a history of adaptation.

121 We next sought to examine the consistency of the simulation results described
122 above using genetic data from a dataset of 230 ancient Eurasian individuals [26].
123 Assuming neutrality, the expected frequency of an allele in contemporary
124 European populations can be predicted as a linear combination of allele
125 frequencies sampled from representative ancient populations that have contributed
126 ancestry to present-day European populations in different proportions [26,27]
127 (Methods). Using this approach, we calculated the expected allele frequency in
128 four present day European samples from the 1,000 Genomes Project [20] at the 11
129 NLS falling within the bounds of the three OAS genes, based on the ancient allele
130 frequencies estimated by Mathieson and colleagues. To set up our null
131 expectations we performed a similar analysis on a dataset of approximately one
132 million SNPs scattered around the genome, generated by Mathieson and
133 colleagues (by merging 213 ancient samples dated between 6,500 and 300 BCE
134 with sequencing data from four European samples from the 1,000 Genomes
135 Project). We found that the NLS at OAS are outliers in the genome with respect to
136 deviations from ancient frequencies. More specifically, we found that the allele
137 frequencies of 6 out of the 11 OAS SNPs tested in the *OAS1-OAS3* region (those 6

138 SNPs fall within the block of SNPs with NLS frequency greater than 99% of
139 neutral simulations) have increased above the frequency predicted by ancient
140 Eurasian samples by more than 20%, significantly more than what we observed for
141 other SNPs genome-wide with comparable present-day frequencies (lowest P =
142 0.00476, Figure 2B, Table S3). Our findings at this single locus are consistent with
143 results from the genome-wide selection scan performed by Mathieson and
144 colleagues [26] where the OAS region also showed evidence of selection ($P < 10^{-7}$
145 , Table S3), even if it did not reach genome-wide significance after multiple-test
146 correction.

147 We next searched for additional evidence of recent selection, as measured by the
148 iHS [28] and DIND [29] statistics. These tests share a similar rationale: an allele
149 that has recently been driven to high population frequency by positive selection
150 should be associated with unusually long-range LD (iHS) and reduced intra-allelic
151 nucleotide diversity (DIND) [28-30]. We found that several NLS in the OAS
152 region show significantly high iHS and DIND values with respect to genome-wide
153 expectations (Figure 3A and S4), further supporting that they have been targeted
154 by positive selection.

155 As an additional means of understanding whether or not Neandertal haplotypes at
156 OAS are longer than would be expected if they had evolved neutrally, we followed
157 up these empirical haplotype-based tests with a simulation approach using a
158 simple test statistic, $H_{D/A}$. This statistic (fully defined in Methods) compares
159 pairwise haplotype homozygosity lengths within the set of haplotypes carrying a

160 derived (Neandertal) allele and within those carrying the ancestral allele. We
161 utilized the same demographic models described above for our frequency-based
162 test to understand whether the haplotypes surrounding derived alleles at NLS are
163 longer than expected under a neutral model, conditional on the map of
164 recombination in the OAS region. Again, we found that several derived
165 Neandertal-like alleles are significantly longer than observed in simulated loci, and
166 that these results were robust to a series of alternative simulation models tested,
167 including the one- and two-pulse models described above and two additional one-
168 pulse models which varied the mutation and recombination rates (Figure 3B, Table
169 S4).

170 Finally, we calculated the levels of population differentiation between European
171 and East Asian populations for all NLS in the OAS region. Interestingly, we found
172 extreme levels of differentiation for most NLS (Fst as high as 0.6, $P_{\text{empirical}} < 0.01$,
173 Figure 3C. Table S5), except within the genomic region covering *OAS1* and part of
174 *OAS3*. These results suggest that NLS surrounding *OAS1* have been positively
175 selected in both European and East Asian populations but that distinct haplotypes
176 have been selected in Europe and Asia.

177 Our population genetic results provide evidence that Neandertal alleles at the OAS
178 locus have likely experienced positive selection during one or several phases after
179 their introduction into the human population, suggesting a possible functional role
180 of these alleles in human innate immune responses. To study this possibility, we
181 analyzed RNA-sequencing data collected on primary macrophages from 96

182 European-descent individuals, before and after *in-vitro* infection with *Salmonella*
183 *typhimurium*. After 2 hours of infection, we found that all OAS genes were
184 strongly up-regulated (up to 19-fold, $P < 1 \times 10^{-10}$, Figure S5), confirming the
185 ability of *Salmonella* to activate the interferon (IFN) production pathway [31-33].
186 Using genotype data available for the same individuals (673 SNPs spanning the
187 OAS region, see methods) we tested if NLS were associated with variation in the
188 expression levels of *OAS1*, *OAS2* or *OAS3,* in either infected or non-infected
189 macrophages. We found that among NLS, individuals that are heterozygous or
190 homozygous for the Neandertal allele show reduced expression levels of OAS3
191 (i.e., they were expression quantitative trait loci, or *cis* eQTL for *OAS3*) (Figure
192 4A, false discovery rate (FDR) < 10%, Table S6). Interestingly, these *cis* eQTL
193 showed a much stronger effect in infected macrophages (best $P_{salmonella} = 3.5\text{x}10^{-3}$
194 *vs* best $P_{\text{non-infected}} = 0.027$), supporting an interaction between the Neandertal
195 haplotype and the *OAS3* response to *Salmonella* infection.

196 In addition to overall changes in expression, we took advantage of the power of
197 RNA-sequencing data to test if NLS in the OAS regions influenced the ratio of
198 alternative isoforms used for each of the OAS genes (i.e., alternative splicing
199 QTL: asQTL). We found that SNPs associated with the Neandertal haplotype are
200 significant asQTL for *OAS1* and *OAS2* in both infected and non-infected
201 macrophages (FDR << 1%; Figure 4B-C). The effect of the splice site variant
202 rs10774671 at determining what isoform is primarily encoded by *OAS1* was
203 particularly strong ($P \leq 2\text{x}10^{-32}$). This SNP is also a strong asQTL and protein
204 QTL in lymphoblastoid cell lines [34,35]. The ancestral G allele at this SNP (A<u>G</u>

205 at acceptor site) retains the splice site whereas the derived allele, A, (AA at
206 acceptor site) disrupts the splice site leading to the usage of a distinct isoform
207 (Figure S6). The Neandertal haplotype harbors the ancestral allele (encoding the
208 p46 isoform), which is associated with high enzyme activity [36]. Interestingly,
209 despite the fact that this ancestral allele is found at ~ 60-70% in most Sub-Saharan
210 African populations, outside of Africa this allele is only found on individuals with
211 the Neanderthal haplotype (with rare exceptions; ~2% of all haplotypes, Figure S2
212 suggesting that the Neandertal segment is effectively reintroducing an ancestral
213 variant that was already present in other human groups. To validate that this SNP
214 had the same impact at determining what *OAS1* isoforms are expressed in African-
215 descent individuals, we analyzed additional RNA-sequencing data collected from
216 41 African-American individuals. As among Europeans, rs10774671 is a strong
217 asQTL for *OAS1* in both non-infected and infected macrophages ($P < 1x10^{-15}$,
218 Figure S7), despite laying in a non-Neandertal haplotype.

219 Because OAS genes are primarily involved in the control of viral infections we
220 decided to validate our functional findings on peripheral blood mononuclear cells
221 (PBMCs) from 40 individuals stimulated/infected with viral-ligands (polyI:C and
222 gardiquimod), and live viruses (Influenza, Herpes simplex virus (HSV) 1 and
223 HSV2). The individuals were chosen based on their genotype for the NLS
224 rs1557866, a SNP that is a strong proxy for the presence or absence of the
225 Neandertal haplotype in the OAS region (9 were homozygous for the Neandertal
226 haplotype, 15 were heterozygous, and 16 homozygous for the modern human
227 sequence).

228 As expected, we found that all viral-associated immune triggers led to a marked
229 increase in *OAS1-3* gene expression levels, as measured by real-time PCR (up to
230 27-fold, $P \leq 1.2x10^{-8}$, Figure 5A), concomitantly with the up-regulation of type-I
231 and type-II interferon genes (Figure S8). Confirming the QTL results obtained in
232 macrophages, we found that rs10774671 was a strong asQTL for *OAS1* in both
233 non-infected and infected PBMCs ($P \leq 4.9x10^{-5}$, Figure 5B). Likewise, we found
234 that the presence of the Neandertal haplotype was associated with reduced
235 expression levels of *OAS3,* particularly in PBMCs infected with influenza (P =
236 $6.1x10^{-3}$) and the synthetic ligand gardiquimod (P =$2.0x10^{-4}$), which mimics a
237 single strand RNA infection (Figure 5B). Interestingly, the Neandertal haplotype
238 harbors additional regulatory variants that only impact expression levels in a cell-
239 type and immune stimuli specific fashion. For example, we found that the
240 Neandertal haplotype is associated with increased expression levels of *OAS2* in
241 non-infected (P=$1.2x10^{-3}$), and gardiquimod-stimulated PBMCs (P=$4.9x10^{-3}$), but
242 neither in macrophages nor in PBMCs treated with other viral agents. Collectively,
243 our functional data provide evidence for a pervasive impact of the Neandertal
244 haplotype on the regulation of *OAS* genes that varies depending on the cell type
245 and the immune stimuli to which the cells are responding.

246 **Discussion**

247 The Neandertal lineage was present in Eurasia for at least 400,000 years [37],
248 providing ample time for Neandertals to adapt to local disease environments. The
249 admixture process, which likely fostered the transmission of pathogens between

250 Neandertals and humans migrating out of Africa, could have also led to the
251 exchange of genes useful in responding to local pathogens. Here, we have
252 demonstrated that a previously reported case of Neandertal introgression at the
253 OAS locus [15] displays signatures of positive selection in the European
254 population. Additionally, we have strengthened the case for adaptive introgression
255 by providing direct functional evidence of a role for the Neandertal OAS
256 haplotype in the regulatory responses in innate immune cells to infectious agents.

257 Our results show that the Neandertal haplotype at OAS is associated with several
258 regulatory variants that reduce expression of *OAS3* in response to infection, as
259 well as encode alternate isoforms of *OAS1* and *OAS2*. These dramatic functional
260 implications of the Neandertal OAS haplotype support our case for adaptive
261 introgression at OAS. Yet, because distinct functional polymorphisms segregate
262 together in the same haplotype, inferring the exact variant(s) targeted by positive
263 selection remains a daunting task. We speculate, however, that one of the strongest
264 direct targets of selection is likely to have been the splice variant identified in
265 *OAS1*.

266 The Neandertal haplotype carries the ancestral allele (G) of the *OAS1* splice
267 variant (rs10774671), which is common both inside and outside of Africa.
268 However, outside of Africa, the only haplotypes carrying this ancestral splice site
269 are closely related to the Neandertal haplotype, with a few exceptions being rare
270 recombined haplotypes (~2% of all haplotypes with the ancestral allele). This
271 pattern reflects the possibility that Neandertal introgression, in effect, served as a

272 means to resurrect the ancestral splice site from local extinction outside of Africa,
273 probably following the out-of-Africa exodus. Interestingly, the same ancestral
274 splice site is found in the Denosivan genome, and may similarly have impacted
275 adaptive introgression into the ancestors of Melanesians. While we cannot at
276 present confirm that the ancestral splice site was missing from the ancestral
277 Eurasian population, the presence of this allele only on the Neandertal haplotype
278 hints at the possibility that this splice site was lost to drift and subsequently re-
279 introduced by Neandertals, providing beneficial genetic variation at the OAS locus
280 (Figure S2). The Neandertal-introgressed allele encodes a protein variant (p46)
281 that is associated with higher enzymatic activity [36]. The adaptive potential of
282 this variant is supported by the observation that this variant (or other variants in
283 strong LD with it) was shown to be associated with: *(i)* reduced infection and
284 replication rates of West Nile virus ([38], but see [39]), *(ii)* improved resistance to
285 hepatitis C virus (HCV) infection [40,41], and *(iii)* variable symptomology of
286 Tick-Borne Encephalitis (TBE) Virus-Induced Disease (homozygous individuals
287 for the Neandertal haplotype show the most severe symptoms of TBE). Strikingly,
288 West Nile, hepatitis C and TBE are all members of the *Flaviviridae* family,
289 suggesting that Flaviviruses might have been the main drivers of selection in
290 *OAS1*.

291 The differential responses of homozygous carriers of the Neandertal OAS
292 haplotype to the different viruses described above suggest that the Neandertal
293 haplotype is not uniformly beneficial in humans. Thus, it is plausible that both
294 spatial and temporal fluctuations in virus populations could have led to fluctuating

295 selection pressure on Neandertal OAS haplotypes, consistent with findings that
296 genes in the immune system have been disproportionately targeted by positive
297 selection since the dawn of agriculture [42].

298 Alternatively, and not mutually exclusively, alleles at OAS, and particularly the
299 *OAS1* splice variant, might be evolving under balancing selection. This hypothesis
300 is supported by the observation that the *OAS1* splice variant (rs10774671) is found
301 at high frequency worldwide (0.11-0.7), and the significantly higher Tajima's D
302 values observed around *OAS1*, as compared to genome-wide expectations (Figure
303 3D). Moreover, *OAS1* is among the most diverse genes in both humans and non-
304 human primates. Indeed, a recent analysis of genome-wide sequence data from a
305 total of 55 individuals from four non-human ape species, chimpanzee (*Pan*
306 *troglodytes ellioti*), bonobo (*Pan paniscus*), gorilla (*Gorilla gorilla gorilla*), and
307 orangutan (*Pongo abelii*), identified *OAS1* as in the top 1% of genes showing the
308 largest levels of nucleotide diversity among ape species, consistent with a scenario
309 of long-term balancing selection (*OAS2* and *OAS3* are ranked in the 60th and 36th
310 percentile of the genome-wide distribution, respectively) or, as previous research
311 has suggested, rapid evolution across the primate order [43]. Further supporting
312 the idea of balancing selection on the introgressed haplotypes, our functional data
313 suggest that the Neandertal haplotype contributes a range of gene expression
314 responses in a cell-type and stimulus-specific manner.

315 Estimates of historical allele frequencies at the OAS locus support the notion that
316 the Neandertal haplotype did not follow a classic selective sweep model with

constant directional selection. Under such a model, the observed present-day frequency of the Neandertal haplotype at the OAS locus of roughly 38% would suggest a codominant fitness effect of $s \sim 0.0014 - 0.0017$, when assuming an initial frequency of 0.02 at introgression approximately 2,000-2,400 generations ago (Methods). However, the observed allele frequency shift of 0.26 over the past 200-340 generations (maximum shift in CEU from ancient samples; see Figure 2B) suggests that the selection coefficient associated with the Neandertal haplotype during this recent human evolution would have been $s \sim 0.0044 - 0.0075$: 2.6-5.4 times larger than the above estimate. Therefore, both temporally varying selection and balancing selection could explain why the Neandertal haplotype at OAS did not show clear signatures of adaptive introgression in previous studies [15,18].

Our study illustrates the difficulty of identifying strong candidates for adaptive introgression. In a genome-wide statistical framework, our use of neutral coalescent simulations as a null distribution for adaptive introgression likely would not have provided significant results after multiple test correction across loci. This suggests that other instances of less obvious adaptive introgression, especially those that did not follow a classic selective sweep model, may remain to be identified. Moving forward, novel methods must be developed to identify such cases. Some progress is now being made on this front. For example, Racimo and colleagues [11] recently developed a genome-wide statistical framework which relies on distributions of uniquely shared derived alleles between humans and Neandertals (as does our study) to identify candidate regions for adaptive

340 introgression. This study also highlighted the OAS locus as a candidate for
341 adaptive introgression. Additionally, estimates of historical allele frequencies with
342 increased spatial and temporal resolution provided by the sequencing of ancient
343 human genomes are likely to play an important role in illuminating candidates for
344 adaptive introgression which do not conform to classical selective sweep models.

345 Conclusions

346 In conclusion, our study demonstrates that the frequency and haplotype
347 distribution of Neandertal-like sites can be used in a neutral simulation framework
348 that accounts for local genomic context to investigate the history of selection at a
349 candidate locus for which genome-wide tests of selection provide ambiguous
350 results. When combined with functional data, our results provide the strongest
351 evidence to date in support of adaptive introgression in the OAS region. More
352 generally, our study raises the possibility that adaptive introgression might not
353 necessarily occur to select newly introduced variants but rather as a means to
354 resurrect adaptive variation in modern human populations that had been lost due to
355 demographic events.

356 Materials and Methods

357 *1. Genome alignments and identification of Neandertal-like sites*

358 Human/chimpanzee ancestral states were computed by parsimony using
359 alignments from the UCSC Genome Browser for the human reference (hg19) and
360 three outgroups chimpanzee (panTro2), orangutan (ponAbe2), and rhesus macaque

361 (rheMac2) [44]. Ancestral state was assumed to be the chimpanzee allele (if
362 available) if its state was confirmed by matching either orangutan or macaque. All
363 sites with no inferred ancestral state were removed from our analysis.

364 We filtered the Altai Neandertal genome [4] and Denisovan genome [3] using the
365 map35_50 set of minimum filters provided at
366 (https://bioinf.eva.mpg.de/altai_minimal_filters/). For the frequency analysis, we
367 combined these filtered datasets with ten samples from outside of Africa (5-Eur
368 European: CEU, FIN, GBR, IBS, TSI; 5-East Asian: CDX, CHB, CHS, JPT,
369 KHB; see Table S7 for population codes) and one sub-Saharan African sample
370 YRI (Yoruba in Ibadan, Nigeria) from the 1000 Genomes Project Phase 3 [20],
371 which we downloaded from
372 (https://mathgen.stats.ox.ac.uk/impute/1000GP%20Phase%203%20haplotypes%2
373 06%20October%202014.html).

374 We first extracted all biallelic variants in our human, Neandertal, and chimpanzee
375 alignments. We considered as Neandertal-like sites (NLS) only those variants
376 where the African sample (YRI) had a derived allele frequency of zero and both
377 the non-African sample and Neandertal carried the derived allele. We restricted
378 the follow-up haplotype based analysis to only the CEU sample. In that analysis
379 we required the derived allele to be present in CEU in at least two copies in order
380 to calculate our haplotype-based test statistic ($H_{D/A}$).

381 *2. Haplotype clustering in the 1000 Genomes Project data*

To assess the relationships and frequencies of Neandertal-like haplotypes in the OAS region, we identified haplotype clusters based on sequence similarity. First, we filtered all 5,008 haplotypes in the 1000 Genomes Project phase 3 dataset to include only SNPs within the bounds of the three OAS genes (hg19 chr12: 113344739-113449528) and at which the Altai Neandertal [4]and Denisovan [3] genomes carry homozygous genotypes. Next, we clustered the human haplotypes such that all haplotypes in a cluster had no more than 60 pairwise differences, which resulted in 10 clusters. We inferred a consensus haplotype for each cluster based on the majority allele at each position in the cluster. Finally, we produced a neighbor-joining tree of the human cluster consensus sequences and the Altai, Denisovan, and ancestral sequences using the R package "ape." We estimated confidence values for nodes with one thousand bootstraps.

We then calculated haplotype frequencies for each of the 1000 Genomes Project population samples based on the assignment of each haplotype to the clusters described above.

3. Demographic model and neutral coalescent simulations

We performed coalescent simulations of the demographic history of the European, East Asian, African, and Neandertal populations applied by Vernot and Akey [25] based on previously inferred demographic models [23,24]. In our first set of simulations, which were performed with ms [45], we extracted only allele frequencies at NLS. We gathered a total of 1 million simulation results. In each simulation run, a result was collected if a NLS was present in either the European

404 or the East Asian population sample (or both). Therefore, null distributions
405 specific to Europeans or East Asians included less than 1 million results (but
406 typically > 800,000). Haplotype simulations were performed with macs [46] in
407 order to explicitly simulate the genetic map (downloaded with the 1000 Genomes
408 samples at the link above) of the 600 kilobase region centered on OAS
409 (chr12:113100000-113700000). The general shape of the demographic model is
410 illustrated in Figure S1. Our baseline simulations were performed with the
411 parameters specified in Table S1, assuming 25 years per generation and a mutation
412 rate of 2.5 x 10^{-8} per bp per generation. Table S1 also provides all parameters used
413 in one- and two- introgression pulse simulations. Additionally, we examined the
414 one-pulse model with a slower mutation rate (1.25 x 10^{-8}) and a one-pulse model
415 with a uniform recombination rate (1.3 x 10^{-8}; a value conservatively lower than
416 the average for the OAS region, 1.7 x 10^{-8}). Sample ms and macs commands are
417 given at the end of this section.

418 For haplotype-based simulations, data were thinned in a manner similar to
419 Sankararaman *et al*. 2014 [6] to account for imperfect SNP ascertainment in the
420 1000 Genomes dataset, such that SNPs with minor allele count of 1, 2, 3, 4, 5, 6, 7,
421 8, 9, and >=10 were accepted with probabilities 0.25, 0.5, 0.75, 0.8, 0.9, 0.95,
422 0.96, 0.97, 0.98, and 0.99, respectively. Additionally, we only kept SNPs that
423 were polymorphic in the simulated CEU sample. Finally, we performed an
424 additional thinning of SNPs with uniform probability of 0.05 of removal to
425 account for slightly elevated SNP density in the simulated data. The resulting
426 simulated datasets had an average SNP density of 3.8 SNPs per kb compared to

2.5 in the real data. This is a slightly larger than ideal difference in SNP density, but we note that neither derived allele frequency, nor our primary haplotype-based test statistic (described below) should be particularly sensitive to SNP density. In fact, Figure S9 illustrates that our statistic is conservative with respect to SNP density. Additionally, our results hold in a simulation with half the mutation rate of our baseline simulation. This simulation resulted in an average SNP density of 1.9 SNPs per kb. So our observation of long haplotypes surrounding NLS is robust to SNP density across our simulations.

Sample ms command:

```
ms 752 1 -s 1 -I 4 250 250 250 2 0 -n 1 58.0027359781 -n 2 70.0410396717 -n 3
187.549931601 -n 4 0.205198358413 -eg 0 1 482.67144247 -eg 0 2
505.592963281 -eg 0 3 720.224280773 -em 0 1 2 0.358619661426 -em 0 2 1
0.358619661426 -em 0 1 3 0.111889334365 -em 0 3 1 0.111889334365 -em 0 2 3
0.446122858814 -em 0 3 2 0.446122858814 -en 0.00699726402189 1
1.98002735978 -eg 0.00699726402189 2 0.0 -eg 0.00699726402189 3
17.5076517287 -en 0.03146374829 2 2.03666547538 -en 0.03146374829 3
0.700185007205 -ej 0.0641347992705 3 2 -em 0.0641347992705 1 2 0.00015 -em
0.0641347992705 2 1 0.00015 -em 0.0839811779742 2 4 0.00075 -em
0.0846651725023 2 4 0 -ej 0.0957592339261 2 1 -en 0.202462380301 1 1.0 -ej
0.957592339261 4 1
```

Sample macs command:

```
macs 416 600000 -t 0.000731 -R oas_recrates.txt -I 4 216 198 0 2 0 -n 1
58.0027359781 -n 2 70.0410396717 -n 3 187.549931601 -n 4 0.205198358413 -
eg 0 1 482.67144247 -eg 1e-12 2 460.409556336 -eg 2e-12 3 720.224280773 -em
3e-12 1 2 0.4441436762 -em 4e-12 2 1 0.4441436762 -em 5e-12 1 3
0.138572826974 -em 6e-12 3 1 0.138572826974 -em 7e-12 2 3 0.552514733193 -
em 8e-12 3 2 0.552514733193 -en 0.00699726402189 1 1.98002735978 -eg
0.00699727402189 2 0.0 -eg 0.00699728402189 3 18.896348561 -en
0.03146374829 2 2.79399962717 -en 0.03146375829 3 0.670250141711 -ej
0.051785044418 3 2 -em 0.051785054418 1 2 0.00015 -em 0.051785064418 2 1
0.00015 -em 0.0555806720117 2 4 0.00075 -em 0.0562646665398 2 4 0 -ej
0.0957592339261 2 1 -en 0.202462380301 1 1.0 -ej 0.957592339261 4 1 -h 1e3
```

4. Frequency and haplotype-based tests of neutrality using simulations

We examined the consistency of genetic variation with our neutral model using several approaches. First, we examined the likelihood of observing (Neandertal) allele frequencies as high as the OAS locus. Under neutrality, allele frequency is not dependent upon recombination rate, therefore, we can estimate the likelihood of our observed NLS frequency in the OAS region. To create a distribution of expected NLS frequency in each introgression model, we first extracted derived allele counts (DAC) at simulated NLS for samples of 250 individuals each for Europeans and East Asians in the simulated model. Next, for each non-African population sample from the 1000 Genomes Project, we binomially sampled the DACs from the appropriate simulated population (European for CEU, GBR, IBS,

470 TSI; East Asian for CDX, CHB, CHS, JPT, KHV) using the true population
471 sample size to create a distribution of NLS frequencies that is specific to each
472 population sample (Figure 2A, S3). Minimum p-values across the OAS locus for
473 each population are listed in Table S2.

474 Additionally, we wanted to examine if the haplotypes carrying NLS at the OAS
475 locus are longer than expected under neutrality when conditioning on the observed
476 frequencies and the underlying genetic map, which would provide an additional
477 signature of selection on introgressed haplotypes beyond empirical haplotype
478 signatures. For this purpose, we modified a simple haplotype statistic *H* [47],
479 which measures the average length of pairwise homozygosity tracts in base pairs –
480 a quantity that is very straightforward to interpret. As selective sweeps are
481 expected to create long haplotypes around the selected site, the *H* statistic should
482 be higher in samples containing positively selected haplotypes compared to
483 samples containing neutrally evolving haplotypes, when frequency and
484 recombination are properly controlled, similar to other statistics based on
485 haplotype lengths, such as *EHH, iHS,* and *nSL* [28,30,48]. However, in contrast to
486 these other statistics, *H* does not require specification of analysis parameters such
487 as minimum haplotype homozygosity levels below which haplotypes are no longer
488 extended.

489 Under adaptive introgression, we specifically expect the introgressed (derived
490 allele carrying) haplotypes to be longer than the ancestral haplotypes, due to the
491 fact that selected Neandertal haplotypes will on average spend less time at low

492 frequency, where they have a greater opportunity for recombination with non-
493 introgressed haplotypes, than neutral Neandertal haplotypes. We therefore defined
494 our test statistic, $H_{D/A}$, as:

495 $$H_{D/A} = \ln(H_D / H_A);$$

496 where H_D and H_A are H calculated across haplotypes carrying derived NLS allele
497 versus the ancestral allele (see Figure S10).

498 For each model we generated 1,000 simulated OAS regions containing NLS that
499 reach a frequency greater than the 99th percentile for CEU in our frequency
500 simulations. We calculated $H_{D/A}$ for every simulated NLS and for every NLS in our
501 true sample. We then compared our simulation results to the observed data in two
502 ways. First, to visually examine the distribution of true $H_{D/A}$ values to neutral
503 simulations, we took the mean $H_{D/A}$ score across all NLS in each of 1,000
504 simulations and calculated the 95th and 99th percentiles of those 1,000 simulations
505 (Figure 3B). Second, to examine the probability under neutrality of the observed
506 $H_{D/A}$ values at the peak of $H_{D/A}$ between chr12:113380000-113420000, we
507 compared the mean $H_{D/A}$ score for SNPs in this window to the mean of SNPs in
508 this window for each simulation that produced a NLS in that window. These
509 results for all tested models are listed in Table S4.

510 *5. Analysis of ancient Eurasian data*

511 We utilized supplementary data table 3 from Mathieson *et al*. [26]. This table
512 includes maximum likelihood allele frequency estimates for three ancient

513 population samples (HG- Hunter-gatherer, EF- Early farmer, SA- Steppe ancestry)
514 and four present day European samples from the 1,000 Genomes Project (see
515 "Genome-wide scan for selection" section of methods in[26]). We intersect this
516 table with allele frequencies for 1,000 Genomes Yorubans (YRI) and the Altai
517 Neandertal genotypes and only analyze sites for which we have data for all
518 samples (1,004,612 SNPs).

519 To calculate the expected allele frequency in modern samples under drift, we used
520 the estimated proportions (*m*) of (HG, EF, SA) in each of the four present-day
521 samples estimated by Mathieson *et al*. [26]: CEU = (0.196, 0.257, 0.547), GBR =
522 (0.362, 0.229, 0.409), IBS = (0, 0.686, 0.314) and TSI = (0, 0.645, 0.355). We
523 calculated the expected frequency E[*p*] of site as:

524 $$E[p] = \sum_{i}^{\{HG,EF,SA\}} (p_i \times m_i)$$

525 Next, we calculated the absolute difference between observed and expected allele
526 frequency in all four present-day European samples at all available sites. To test
527 the null hypothesis that OAS NLS have not changed in frequency more than
528 expected under neutrality at 11 SNPs in the central OAS region
529 (chr12:113200000-113600000), we first calculated the fraction of all autosomal
530 SNPs in the dataset at similar present-day frequency (within 1 percent in the
531 folded frequency spectrum) of each OAS NLS. Finally, we calculated the fraction
532 of autosomal SNPs with an absolute observed minus expected frequency

difference greater than or equal to the OAS NLS. These results are given in Table S3 and illustrated in Figure 2B.

This test does not explicitly incorporate variance in estimated ancient allele frequency. However, any bias in ancient allele frequency estimation should be distributed randomly across the genome. Therefore, our comparison to a genome-wide distribution of SNPs at similar present-day frequency should incorporate most of this error. Nonetheless, the selection test performed by Mathieson *et al.* [26] does incorporate such error, so we can also look to the Ps from that test to ensure consistency with our results.

6. Estimation of selection coefficients

To estimate the selection coefficient s under constant positive selection for a given starting frequency (x_0), final frequency (x_1), and number of generations between these estimates (Δt), we assumed a model of standard logistic growth of a codominant allele:

$$x_1 = \frac{x_0}{x_0 + (1 - x_0)e^{-s\Delta t}}$$

This equation can be easily solved to obtain s, given x_0 , x_1, and Δt.

7. Probabilities that Neandertal haplotypes are shared due to incomplete lineage sorting

551 We estimated the probability that Neandertal haplotypes observed in the OAS
552 region could be a product of ILS using the method outlined by Huerta-Sanchez *et*
553 *al*. [49]. This method estimates the probability that a haplotype of length (H) is
554 shared due to incomplete lineage sorting as:

555 *P(H) = 1 - gammaCDF(H, shape = 2, rate = 1/L) ;*

556 where L is the expected shared length, L = 1/(r x t) where r is recombination rate
557 and t is time in generations.

558 We first estimated the maximum haplotype length observed in each of the 1000
559 Genomes Project population samples by identifying tracts of identity-by-state
560 (IBS) that include NLS between the Altai Neandertal haplotype (considering only
561 homozygous positions) and individual human haplotypes. We identified all tracts
562 of IBS bounded by NLS (using YRI as the African reference) and took the
563 maximum of these per-population sample IBS distributions.

564 We identified the maximum tract length (198,441 bp) in European (and some
565 admixed Native American) samples. Maximum tract length for East Asian
566 samples (54,385 bp) is notably shorter. As expected, no IBS tracts were identified
567 in African population samples.

568 Assuming a conservatively low recombination rate for the OAS region (1.3×10^{-8})
569 and a conservatively short divergence between Neandertals and humans of 300
570 thousand years (and 25 years per generation), the probability of a length of at least
571 54,385 is P(54385) = 0.002. The probability of the longest tracts is much smaller,

572 P(198441) = 1.15 x 10^{-12}. Therefore, it is unlikely that Neandertal haplotypes are
573 shared with non-Africans due to shared ancestral variation.

574 We repeated this analysis using the Denisovan genome and found no IBS tracts
575 defined by Denisovan-like sites, suggesting that introgressed Denisovan
576 haplotypes described by Mendez *et al*. [17] are not present in the 1000 Genomes
577 Project Samples, consistent with our findings in Figure 1A.

578 *8. Neutrality tests in phase 3 of the 1000 Genomes data.*

579 We calculated iHS, DIND, Fst and Tajima's D on different populations from
580 phase 3 of the 1000 Genomes project. The phased data were downloaded from
581 Impute reference data panel
582 (https://mathgen.stats.ox.ac.uk/impute/1000GP_Phase3.html) and were filtered for
583 biallelic SNPs. Arlequin version 3.5.1.3 [50] was then used to calculate Fst
584 estimates derived from ANOVA among all pairs of European and Asian
585 populations. DIND was calculated as previously described [29] and Tajima's D
586 was calculated for all SNPs using a window of 25kb either side of each SNP (i.e.,
587 in window of 50kb in total). iHS values were recovered from a genomic scan
588 performed using hapbin [51] on the same phase 3 release of the 1000 Genomes
589 dataset.

590 9. *Sample collection*

591 Buffy coats from 96 healthy European American donors and 41 African
592 Americans were obtained from Indiana Blood Center (Indianapolis, IN, USA).

593 Only individuals self-reported as currently healthy and not under medication were
594 included in the study. The project was approved by the ethics committee at the
595 CHU Sainte-Justine (protocol #4022). The individuals recruited in this study were
596 males aged 18 to 55 years old. For 80% of our samples we have information on
597 their exact age (for the remaining 20% of donors we only know that they were
598 adults less than 55 years old), and we found no association between the presence
599 of the Neandertal haplotype (as measure by rs1557866) and age ($P > 0.5$). Thus,
600 variation in age is not likely impact any of our conclusions. In addition to self-
601 identifed ancestry labels, we used the genome-wide genotype data (see section 10)
602 to estimate genome-wide levels of European and African ancestry in each sample
603 using the program ADMIXTURE [52]. Consistent with previous reports, we found
604 that self-identified EA showed limited levels of African admixture (mean= 0.4%,
605 range 0-13%). The African Americans used in our study were selected on having
606 at least 75% of African ancestry.

607 *10. DNA Extraction and genotyping*

608 DNA from each of the blood donors was extracted using the Gentra Pure Gene
609 blood kit (Qiagen). Genotyping of each individual was then performed by
610 Illumina's HumanOmni5Exome bead Chip array and complemented with imputed
611 data from the 1000 Genomes data using Impute2 [53]. Here, we only focused on
612 genetic diversity surrounding the OAS region – chr12:113229549-113574044 (~
613 344Kb) spanning from the beginning of *RPH3A* to the end of *RASAL1* – for a total
614 of 673 SNPs with a MAF above 10%. Genotypes can be found in Table S8.

615 *11. Isolation of monocytes and differentiation of macrophages*

616 Blood mononuclear cells were isolated by Ficoll-Paque centrifugation. Monocytes
617 were purified from peripheral blood mononuclear cells (PBMCs) by positive
618 selection with magnetic CD14 MicroBeads (Miltenyi Biotech) using the
619 autoMACS Pro Separator. All samples had purity levels above 90%, as measured
620 by flow cytometry using an antibody against CD14 (BD Biosciences). Monocytes
621 were then cultured for 7 days in RPMI-1640 (Fisher) supplemented with 10%
622 heat-inactivated FBS (FBS premium, US origin, Wisent), L-glutamine (Fisher)
623 and M-CSF (20ng/mL; R&D systems). Cell cultures were fed every 2 days with
624 complete medium supplemented with the cytokines previously mentioned. Before
625 infection, we systematically verified that the differentiated macrophages presented
626 the expected phenotype for non-activated macrophages (CD1a+, CD14+, CD83−,
627 and HLA-DRlow (BD Biosciences)).

628 *12. Bacterial preparation and infection of macrophages*

629 The day prior to infection, aliquots of *Salmonella typhimurium* (Keller strain) were
630 thawed and bacteria were grown overnight in Tryptic Soy Broth (TSB) medium.
631 Bacterial culture was diluted to mid-log phase prior to infection and supernatant
632 density was checked at OD600. Monocyte-derived macrophages were then
633 infected with *Salmonella typhimurium* at a multiplicity of infection (MOI) of 10:1.
634 A control group of non-infected macrophages was treated the same way but using
635 medium without bacteria. After 2 hours in contact with the bacteria, macrophages
636 were washed and cultured for another hour in the presence of 50 mg/ml of

637 gentamycin in order to kill all extracellular bacteria present in the medium. The
638 cells were then washed a second time and cultured in complete medium with 3
639 mg/ml gentamycin for an additional 2 hours, the time point to which we refer in
640 the main text.

641 *13. Infection/stimulation of PBMC*

642 PBMCs from a subset of 40 individuals used to derive macrophages were cultured
643 in RPMI-1640 (Fisher) supplemented with 10% heat-inactivated FBS (FBS
644 premium, US origin, Wisent) and 1% L-glutamine (Fisher). The 30 individuals
645 were chosen based on their genotype for rs1557866, a SNP which derived allele is
646 of Neandertal origin and that we used as a proxy to identify individuals harbouring
647 the Neandertal haplotype in the OAS region. From the 40 individuals, and based
648 on this SNP, 9 individuals were homozygous for the Neandertal haplotype, 15
649 were heterozygous, and 16 homozygous for the modern human sequence.

650 For each of the tested individuals, PBMCs (1 million per condition) were
651 stimulated/infected with one of the following viral-associated immune challenges:
652 polyI:C (10 μg/ml, TLR3 agonist), gardiquimod (0.5μg/ml, TLR7 and TLR8
653 agonist), Influenza PR8 WT (multiplicity of infection (MOI) of 0.05:1), Herpes
654 simplex virus (HSV) 1 ($1.55x10^2$ CPE), and HSV2 ($19.5x10^4$ CPE). PBMCs were
655 stimulated/infected for 4 hours with TLR ligands and Influenza, and 6h with
656 HSV1 and HSV2. A control group of non-infected PBMC was treated the same
657 way but with only medium.

658 *14. RNA extraction, RNA-seq library preparation, and sequencing*

659 Total RNA was extracted from the non-infected and infected/stimulated cells
660 using the miRNeasy kit (Qiagen). RNA quantity was evaluated
661 spectrophotometrically, and the quality was assessed with the Agilent 2100
662 Bioanalyzer (Agilent Technologies). Only samples with no evidence of RNA
663 degradation (RNA integrity number > 8) were kept for further experiments. RNA-
664 sequencing libraries were prepared using the Illumina TruSeq protocol. Once
665 prepared, indexed cDNA libraries were pooled (6 libraries per pool) in equimolar
666 amounts and sequenced with single-end 100bp reads on an Illumina HiSeq2500.
667 Results based on the entire dataset are described elsewhere (Nédélec *et al*., under
668 revision). Here, we only studied transcript-level and gene-level expression
669 estimates for *OAS1*, *OAS2* and *OAS3*. The transcript-level and gene-level
670 expression data for these genes can be found in Table S9.

671 *15. Quantifying gene expression values from RNA-seq data*

672 Adaptor sequences and low quality score bases (Phred score < 20) were first
673 trimmed using Trim Galore (version 0.2.7). The resulting reads were then mapped
674 to the human genome reference sequence (Ensembl GRCh37 release 65) using
675 TopHat (version 2.0.6) and using a hg19 transcript annotation database
676 downloaded from UCSC. Gene-level expression estimates were calculated using
677 featureCounts (version 1.4.6-p3) and transcript-level expression values were
678 obtained using RSEM under default parameters.

679 *16. Quantitative real time PCR*

680 For the PBMC samples we measured the expression levels of OAS and interferon
681 genes using real time PCR. 100ng of high-quality RNA was reverse-transcribed
682 into cDNA using the qScript cDNA SuperMix (Quanta Biosciences). Quantitative
683 real time PCR was performed using 96.96 Dynamic Array™ IFCs and the
684 BioMark™ HD System from Fluidigm. For the TaqMan gene assays, we used the
685 following TaqMan Gene Expression Assay (Applied BioSystems) to quantify the
686 expression levels of interferon genes: *IFNA1* (Hs03044218), *IFNA6*
687 (Hs00819627), and *IFNG* (Hs00989291). To quantify the overall expression levels
688 of OAS genes, we used probes that capture all common isoforms of *OAS1*
689 (Hs00973635), *OAS2* (Hs00942643), and OAS3 (Hs00196324). Custom-made
690 probes were designed to specifically target the short-isoform of *OAS2* (Forward
691 Primer Sequence CTGCAGGAACCCGAACAGTT; Reverse Primer Sequence
692 ACTCATGGCCTAGAGGTTGCA; Reporter Sequence
693 AGAGAAAAGCCAAAGAA). As housekeeping genes we used: *GAPDH*
694 (Hs02758991), *GUSB* (Hs99999908), *HPRT1* (Hs99999909), and *POLR2A*
695 (Hs00172187). The results reported in the manuscript used *POLR2A* as a reference
696 but all conclusions remain unchanged when using any of the other housekeeping
697 genes.

698 We start by doing a preamplification of the cDNA using the PreAmp Master Mix
699 (Fluidigm). Preamplified cDNA was then diluted 2X on a solution of 10 mM Tris–
700 HCl (pH 8.0) and 0.1 mM EDTA. In order to prepare samples for loading into the
701 integrated fluid circuit (IFC), a mix was prepared consisting of 360 μL TaqMan

702 Fast Advanced Master Mix (Applied BioSystems) and 36 μL 20× GE Sample
703 Loading Reagent (Fluidigm). 2.75 μL of this mix was dispensed to each well of a
704 96-well assay plate and mixed with 2.25 μL of preamplified cDNA. Following
705 priming of the IFC in the IFC Controller HX, 5 μL of the mixture of cDNA and
706 loading reagent were dispensed in each of the sample inlet of the 96.96 IFC. For
707 the TaqMan gene assays, 5 μL of mixes consisting of 2.5 μL 20× TaqMan Gene
708 Expression Assay (Applied BioSystems) and 2.5 μL 2X Assay Loading Reagent
709 (Fluidigm) were dispensed to each detector inlet of the 96.96 IFC. After loading
710 the assays and samples into the IFC in the IFC Controller HX, the IFC was
711 transferred to the BioMark HD and PCR was performed using the thermal protocol
712 GE 96 × 96 Fast v1.pcl. This protocol consists of a Thermal Mix of 70 °C, 30 min;
713 25 °C, 10 min, Hot Start at 95 °C, 1 min, PCR Cycle of 35 cycles of (96 °C, 5 s;
714 60 °C, 20 s). Data was analysed using Fluidigm Real-Time PCR Analysis software
715 using the Linear (Derivative) Baseline Correction Method and the Auto
716 (Detectors) Ct Threshold Method.

717 To quantify the expression levels of the *OAS1* isoform associated with the derived
718 allele at the splicing variant rs10774671 we used SybrGreen and the following
719 forward (GCTGAGGCCTGGCTGAATTA), and reverse
720 (CCACTTGTTAGCTGATGTCCTTGA) primers. PCR was performed using the
721 thermal protocol 50 °C, 2 min; 95 °C, 10 min, PCR Cycle of 40 cycles of (95 °C,
722 15 s; 60 °C, 1 min). A melting curve was also performed to check for non-specific
723 amplification.

724 *17. Genotype–Phenotype Association Analysis*

725 eQTL, asQTL were performed against *OAS1*, *OAS2* and *OAS3*. We examined
726 associations between SNP genotypes and the phenotype of interest using a linear
727 regression model, in which phenotype was regressed against genotype. In
728 particular, expression levels were considered as the phenotype when searching for
729 eQTL and the percentage usage of each isoform in each gene when mapping
730 asQTL. To avoid low power caused by rare variants, only SNPs in the OAS region
731 with a minor allele frequency of 10% across all individuals were tested (i.e., 673
732 SNPs within the region chr12:113229549-113574044). In all cases, we assumed
733 that alleles affected the phenotype in an additive manner. For the eQTL and
734 asQTL analyses on macrophages we mapped Salmonella-infected, and non-
735 infected samples separately. We controlled for false discovery rates (FDR) using
736 an approach analogous to that of Storey and Tibshirani[54], which makes no
737 explicit distributional assumption for the null model but instead derives it
738 empirically null from permutation tests, where expression levels were permuted
739 1000 times across individuals. For the non-infected and infected/stimulated
740 PBMCs we only tested expression levels against the SNPs identified as eQTL or
741 asQTL in the macrophage data (specifically, the SNPs for which boxplots are
742 shown in Figure 4).

743 **Author Contributions:** Conception and design: AJS, PWM, LBB; Acquisition of
744 data: AJS, AD, YN, VY, LBB; Analysis and interpretation of data: AJS, AD, YN,
745 PWM, LBB; Contributed unpublished, essential data, or reagents: CA, JET;
746 Drafting or revising the article: AJS, PWM, LBB.

Acknowledgements: We thank all members from the Barreiro and Messer labs for helpful discussions and comments on the manuscript. We thank Dr. Silvia Vidal for the gift of the Influenza PR8 WT used in this study, Dr. Hugo Soudeyns and Doris Ransy for advice with the viral infections, and Marc Montero and George (PJ) Perry for sharing their analysis on nucleotide diversity levels of OAS genes in non-human primate species.

Availability of data and materials: The datasets supporting the conclusions of this article are included within the article and in supplementary Tables 8 and 9. The raw data were deposited under GEO accession numbers GSE73765 and GSE81046.

Competing interests: The authors declare that they have no competing interests.

Funding Statement: This study was funded by grants from the Canadian Institutes of Health Research (301538 and 232519), the Human Frontiers Science Program (CDA-00025/2012) and the Canada Research Chairs Program (950-228993) (to L.B.B.). Y.N. was supported by a fellowship from the *Réseau de Médecine Génétique Appliquée* (RMGA).

Figures:

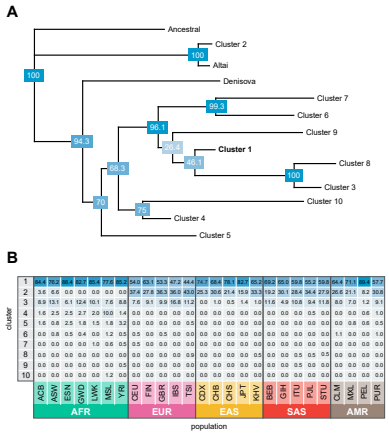

Figure 1: Neandertal introgresssed haplotypes in the OAS region. (A) Neighbor-joining tree of 5008 phased haplotypes spanning chr12: 113344739-113449528 (hg19) from phase 3 of the 1000 Genomes Project. Haplotypes were condensed into 10 core haplotypes based on the majority allele after clustering into groups of haplotypes with pairwise differences of 60 or less. The figure illustrates that the Altai haplotype is very similar to "cluster 2" haplotypes found in several human populations, while the Denisovan haplotype is not more closely related to any of the remaining (non-cluster 2) sequences in this dataset. Bootstrap values (1000 replicates) are provided in blue boxes at each node. (B) Frequencies of the 10 core haplotypes within each 1000 Genomes Project population sample. The most common Neandertal-like haplotype, cluster 2, is found only outside of sub-Saharan African samples, with the exception of recently admixed populations. Population codes can be found in Table S7.

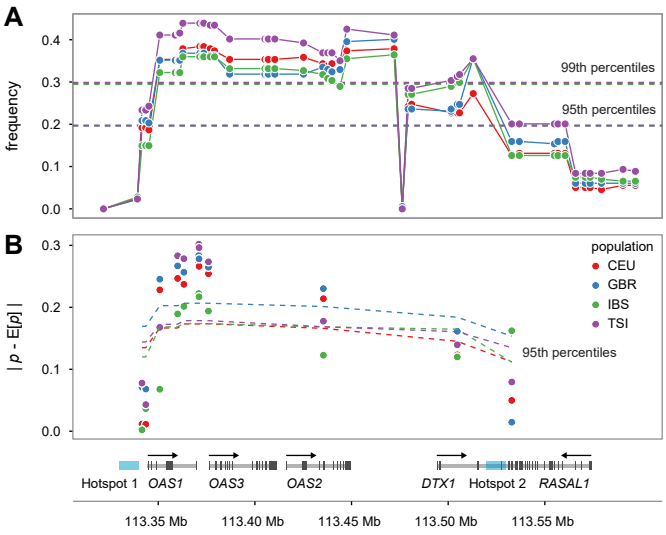

Figure 2: OAS-introgressed haplotypes are found at higher frequencies in European populations than expected under neutrality. (A) Comparison of frequency (y-axis) of NLS in the OAS locus in the CEU, GBR, IBS, and TSI European population samples with respect to neutral expectations (dashed lines) based on coalescent simulations. (B) Absolute difference between observed and expected allele frequency in the same four present-day European samples (y-axis) based on ancient DNA data. Dashed lines represent the 95th percentile of the expected distribution based on similar deviations calculated on a dataset of approximately one million SNPs scattered around the genome and with comparable present-day frequencies to those found for NLS in the OAS region.

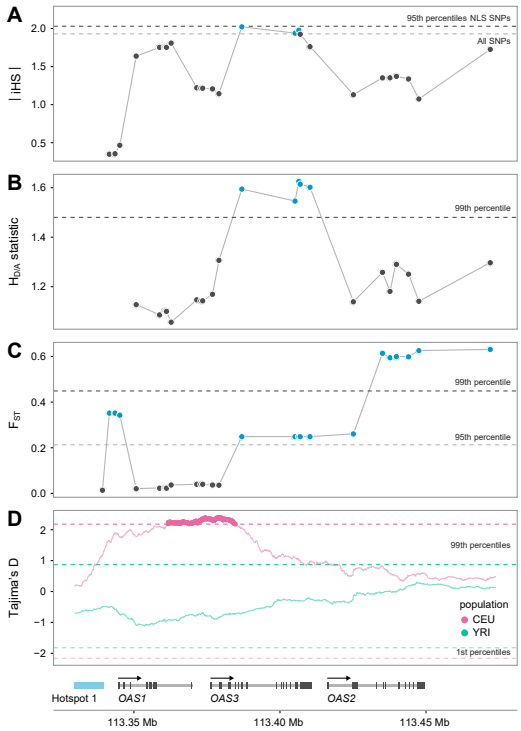

Figure 3: OAS-introgressed haplotypes show multiple signatures of positive selection. (A) Normalized absolute iHS scores (y-axis) across SNPs in the CEU sample. Dashed lines represent the 95th percentile of iHS calculated genome-wide across all SNPs (grey) and all NLS SNPs (black). (B) The $H_{D/A}$ statistic in CEU (y-axis). Dashed line indicates the 99th percentile of $H_{D/A}$ calculated across 1,000 simulations. (C) Fst calculated between CEU and all East Asian populations from the 1000 Genomes projects (y-axis). Dashed lines indicate the 95th (grey) and 99th (black) genome-wide percentiles of Fst. Similar results are obtained when comparing any other European population against East Asians (Table S5). (D) Tajima's D (y-axis) calculated for CEU and YRI samples. Dashed lines indicate the 1st and 99th genome-wide percentiles of Tajima's D.

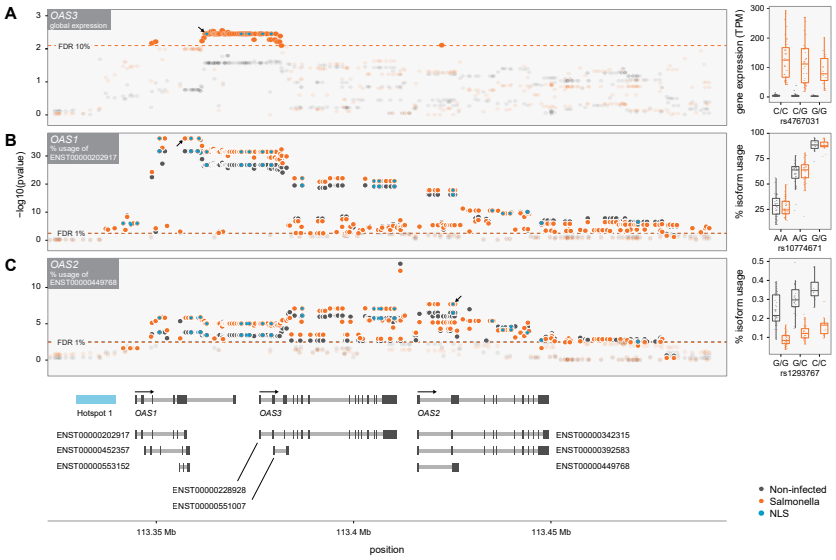

Figure 4: Pervasive impact of the Neandertal haplotype on the regulation of *OAS* genes in primary macrophages. (A) –log 10 Ps (y-axis) for the association between genotypes for SNPs with a MAF > 10% in the OAS region and expression levels of *OAS3* in non-infected (black) and Salmonella-infected macrophages (orange). The dashed line shows the P cutoff corresponding to an FDR of 10%. The right panel shows a boxplot for the association between genotypes at the NLS rs4767031 (x-axis) and the expression levels of *OAS3* in TPM (Transcripts Per Kilobase Million) (y-axis). The lower expression level of *OAS3* in individuals harboring the Neandertal haplotype were confirmed by real-time PCR (Figure S11) (B) –log 10 Ps (y-axis) for the association between genotypes in the OAS regions and the percentage usage of isoform ENST00000202917 (i.e., p46 in the text) in non-infected (black) and Salmonella-infected macrophages (orange). The dashed line shows the P cutoff corresponding to an FDR of 1%. The right panel shows a boxplot for the association between genotypes at the splicing variant rs10774671 (x-axis) and the percentage usage of isoform p46 (y-axis). (C) Similar

824 to (B) but for the percentage usage of isoform ENST00000449768 of OAS2. In all
825 the panels NLS are highlighted by blue dots. The arrows on panel A-C highlight
826 the location of the SNPs for which the boxplots are shown on the right.
827
828
829
830
831
832
833
834
835
836
837

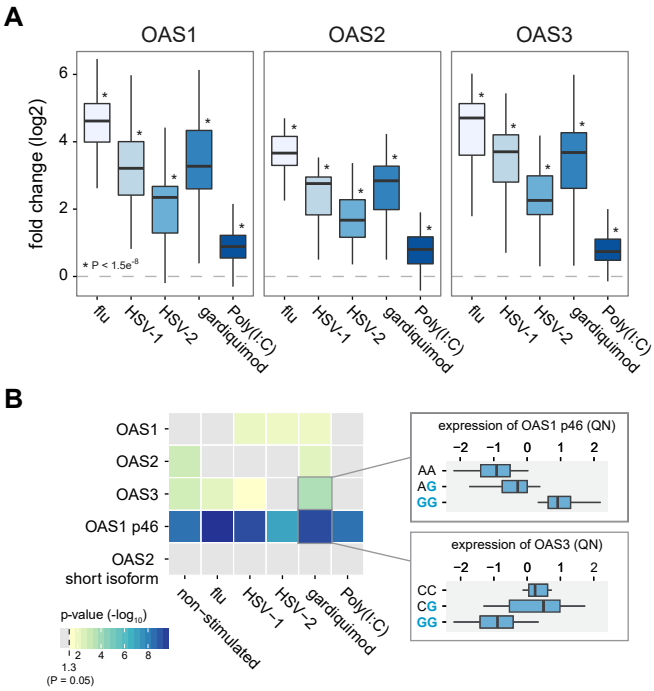

Figure 5: The Neandertal haplotype in the OAS regions has a different impact on the regulation of OAS genes depending on the viral agents PBMCs are exposed to. (A) Log 2 fold induction (y-axis) of *OAS1*, *OAS2* and *OAS3* in response to different viral agents or viral-associated immune stimuli, relative to non-infected PBMCs (B) –log10 P for the association between genotype status for the Neandertal haplotype and overall expression levels of OAS genes and the expression of specific isoforms of *OAS1* and *OAS2* (those identified in Figure 3 as associated with NLS). Boxplots show the association between genotype status (blue referring to Neanderthal alleles) and expression levels of the p46 isoform of *OAS1* and *OAS3* in Gardiquimod-stimulated PBMCs.

852 **Supplementary Figures:**

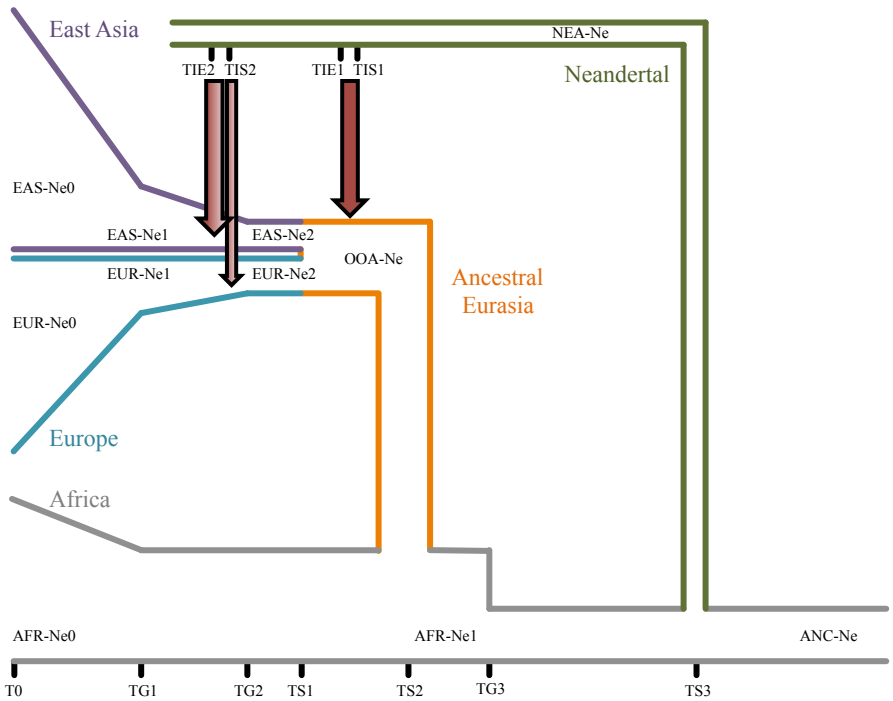

853

854 **Figure S1:** Schematic representation of demographic model used in simulations.

855 Red arrows indicate points of introgression. The full range of demographic

856 parameters used for the simulation can be found in Table S1.

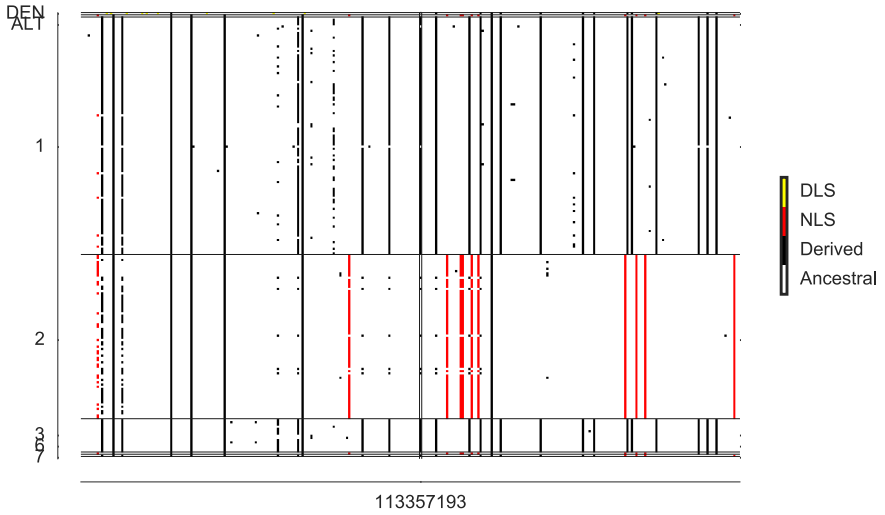

857

858 **Figure S2:** Haplogram of region surrounding *OAS1* splice site (rs10774671). 198
859 phased haplotypes from the CEU population sample are illustrated along with the
860 Altai and Denisovan haplotypes. Ancestral alleles are colored white, derived
861 alleles are (1) yellow if derived in Denisovan and absent from Africans (YRI)
862 (DLS), (2) red if derived in Neandertals and absent from Africans (YRI) (NLS),
863 (3) black otherwise. With the exception of two rare haplotypes in cluster 1, all
864 occurrences of the ancestral variant at rs10774671 are surrounded by derived
865 Neandertal alleles, indicating that these were introduced in a Neandertal
866 haplotype. Only sites where the Neandertal and Denisovan genomes are
867 homozygous were used in this haplogram. Cluster labels (y-axis) correspond to
868 clusters in Figure 1.

869

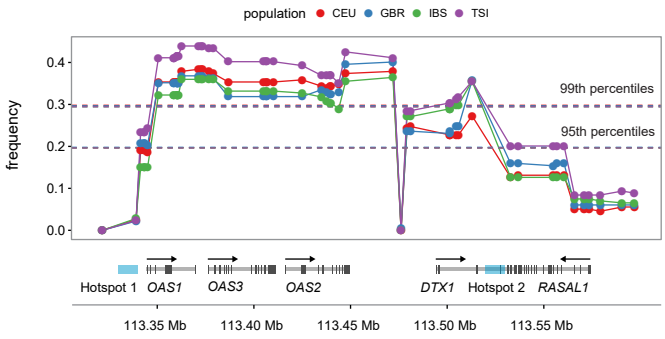

Figure S3: OAS-introgressed haplotypes are found at higher frequencies in European populations than expected under neutrality when using a two-pulse introgression model. (A) Comparison of frequency (y-axis) of NLS in the OAS locus in the CEU, GBR, IBS, and TSI European population samples with respect to neutral expectations (dashed lines) based on coalescent simulations considering two-pulse introgression in both Europeans and Asians, or a second pulse of introgression only in Europeans. Dashed lines overlap almost completely, reflecting little variation between a two-pulse introgression in both European and Asians, or a second pulse only in Europeans.

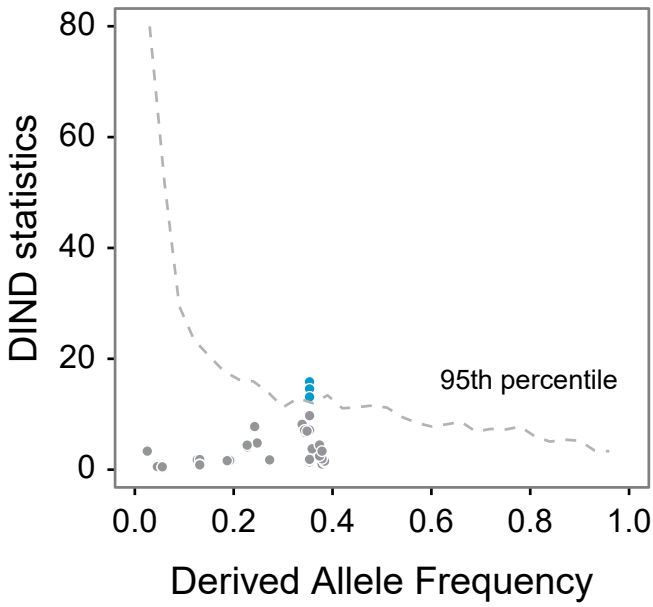

886

887 **Figure S4:** The DIND statistic indicates reduced diversity surrounding NLS.

888 DIND (y-axis) is plotted for SNPs in OAS locus by derived (Neandertal) allele

889 frequency. Dashed line indicates genome-wide 95th percentile by frequency.

890

891

892

893

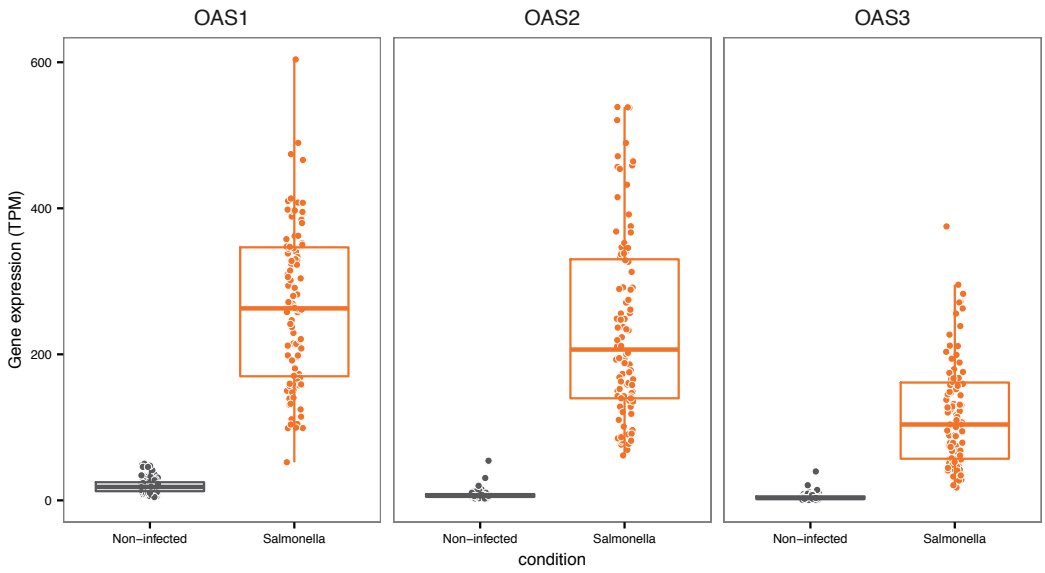

894

895 **Figure S5:** Expression levels of OAS genes in primary macrophages (European)

896 before and after infection with Salmonella.

897

898

899

900

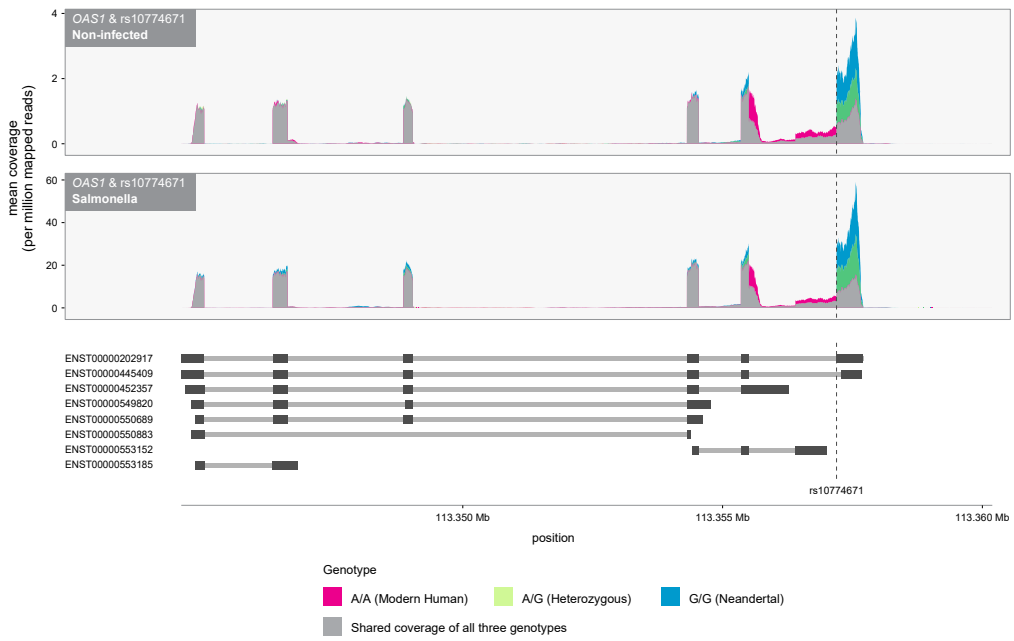

Figure S6: The splicing variant rs10774671 is a strong asQTL for *OAS1*. Plotted is the normalized average coverage at which each base was sequenced along the genomic regions encoding the gene *OAS1*. Individuals were stratified according to their genotype at rs10774671. Below the figure are gene models from the Ensembl database. Individuals carrying the G allele at rs10774671 (i.e. the Neandertal allele) primarily express the transcript ENST00000202917 (referred to as p46 in the text) whereas individuals carrying the A derived allele lose the splice site, which leads to the usage of a distinct isoform.

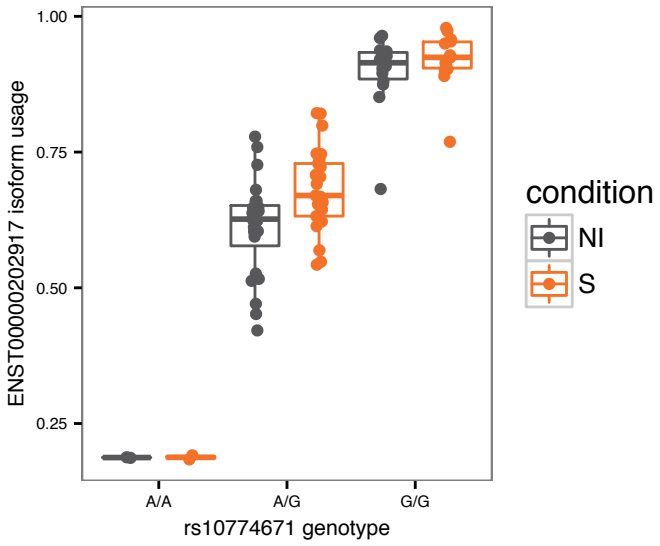

910

911 **Figure S7:** Isoform usage for transcript ENST00000202917 stratified by

912 genotype at rs10774671 in cells derived from individuals with African ancestry.

913 The derived (Neandertal) allele leads to increased expression of

914 ENST00000202917 in both non-infected and *Salmonella* infected conditions.

915

916

917

918

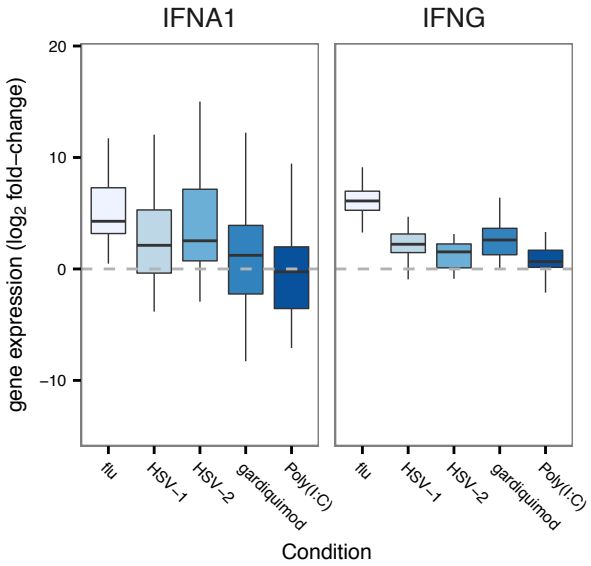

Figure S8: Log 2 fold induction (y-axis) of IFNA1 (type 1 interferon) and IFNG (type II interferon) in PBMCs upon stimulation with several viral agents.

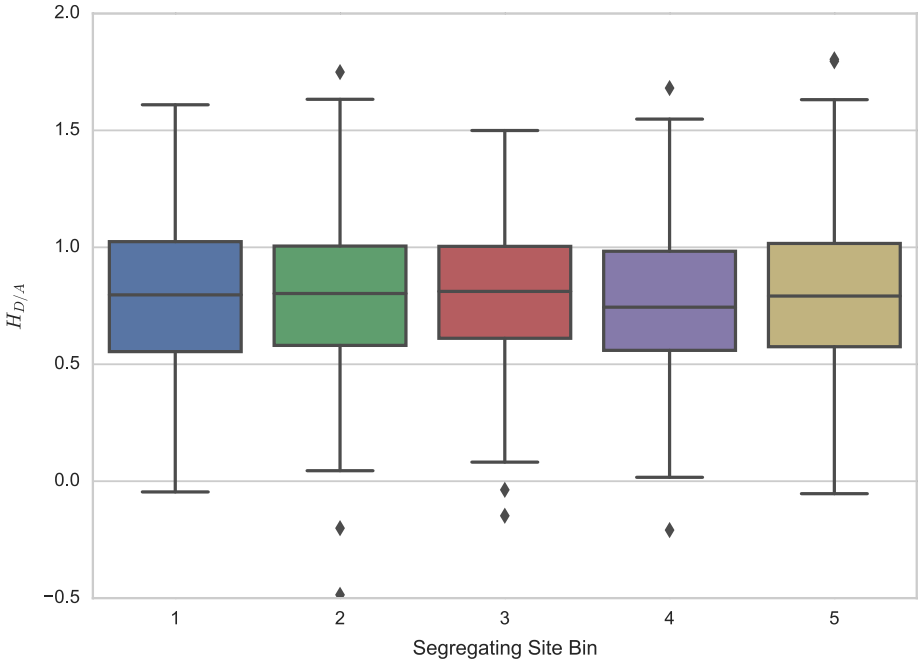

Figure S9: $H_{D/A}$ plotted against quintiles of segregating sites in 1,000 simulations. The $H_{D/A}$ statistic does vary with number of segregating sites across simulated data.

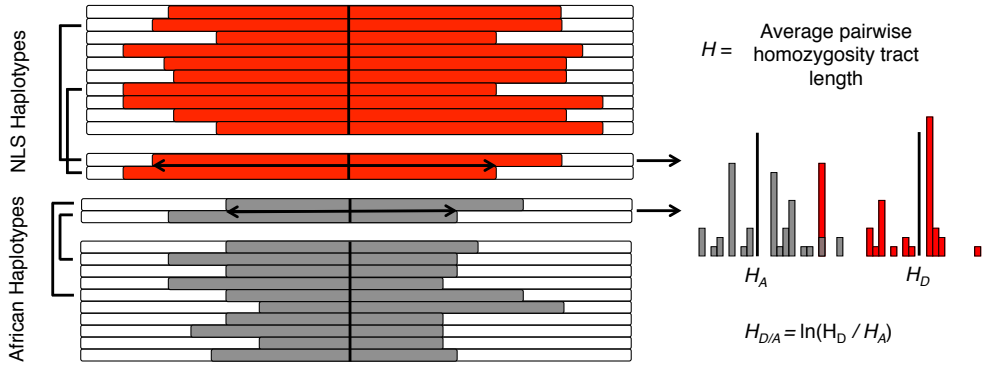

933

934 **Figure S10:** Schematic illustration of the $H_{D/A}$ statistic. At each NLS, haplotypes

935 are divided into two groups, based on whether they carry the Neandertal (derived)

936 or African (ancestral) state. Within each haplotype subset, haplotype

937 homozygosity is calculated across all pairs of haplotypes and then averaged (H),

938 resulting in two values; H_A and H_D (A-ancestral, D-derived). Finally, $H_{D/A}$ is

939 calculated as the natural log of the ratio of derived to ancestral H values.

940 Excessively high values of this statistic reflect particularly long haplotypes

941 carrying Neandertal-derived alleles.

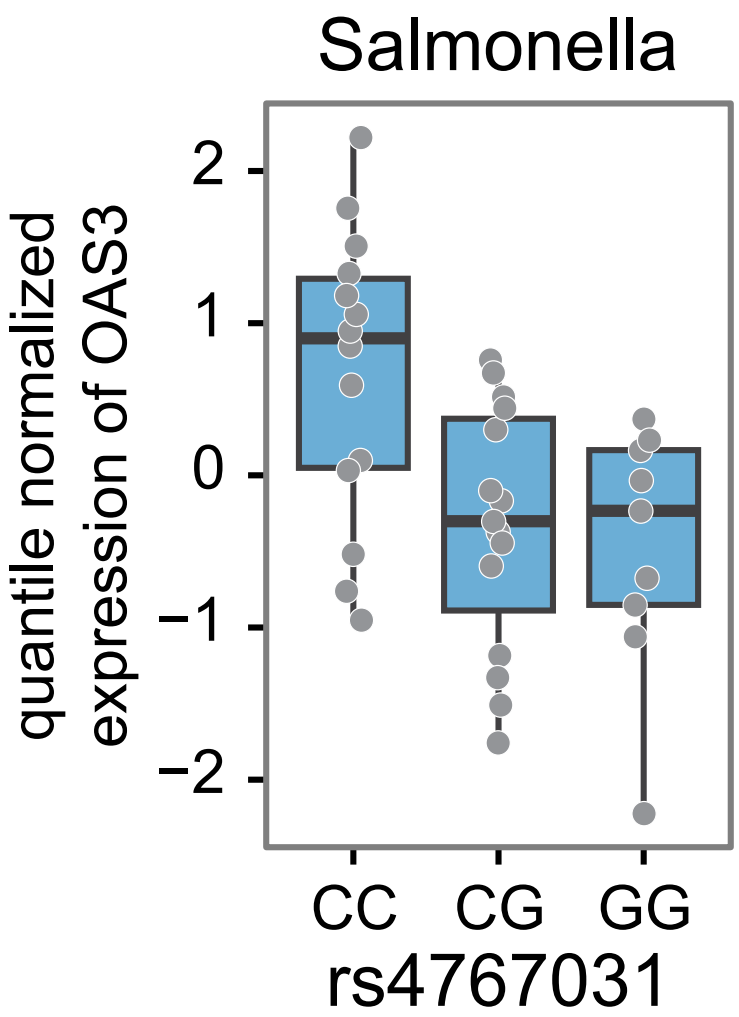

Figure S11: Boxplot for the association between genotypes at the NLS rs4767031 (x-axis) and the expression levels of *OAS3* in *Salmonella*-infected macrophages using real-time PCR.

References:

1. Green RE, Krause J, Briggs AW, Maricic T, Stenzel U, Kircher M, et al. A draft sequence of the Neandertal genome. Science. American Association for the Advancement of Science; 2010;328:710–22.

2. Reich D, Green RE, Kircher M, Krause J, Patterson N, Durand EY, et al. Genetic history of an archaic hominin group from Denisova Cave in Siberia. Nature. Nature Publishing Group; 2010;468:1053–60.

3. Meyer M, Kircher M, Gansauge MT, Li H, Racimo F, Mallick S, et al. A high-coverage genome sequence from an archaic denisovan individual. Science. American Association for the Advancement of Science; 2012;338:222–6.

4. Prüfer K, Racimo F, Patterson N, Jay F, Sankararaman S, Sawyer S, et al. The complete genome sequence of a Neanderthal from the Altai Mountains. Nature. 2014;505:43–9.

5. Sawyer S, Renaud G, Viola B, Hublin J-J, Gansauge M-T, Shunkov MV, et al. Nuclear and mitochondrial DNA sequences from two Denisovan individuals. Proceedings of the National Academy of Sciences. National Acad Sciences; 2015;:201519905.

6. Sankararaman S, Mallick S, Dannemann M, Prüfer K, Kelso J, Pääbo S, et al. The genomic landscape of Neanderthal ancestry in present-day humans. Nature. 2014;507:354–7.

7. Llorente MG, Jones ER, Eriksson A, Siska V, Arthur KW, Arthur JW, et al. Ancient Ethiopian genome reveals extensive Eurasian admixture throughout the African continent. Science. 2015.

8. Vernot B, Akey JM. Resurrecting surviving Neandertal lineages from modern human genomes. Science. 2014;343:1021.

9. Harris K, Nielsen R. The Genetic Cost of Neanderthal Introgression. Genetics. Genetics; 2016;:genetics.116.186890.

10. Racimo F, Sankararaman S, Nielsen R, Huerta-Sanchez E. Evidence for archaic adaptive introgression in humans. Nat Rev Genet. Nature Publishing Group; 2015.

11. Racimo F, Marnetto D, Huerta-Sanchez E. The landscape of uniquely shared archaic alleles in present-day human populations. bioRxiv. Cold Spring Harbor Labs Journals; 2016;:045237.

12. Hublin JJ. The origin of Neandertals. Proceedings of the National Academy of

982 Sciences. 2009;106:16022–7.

983 13. Ségurel L, Quintana-Murci L. Preserving immune diversity through ancient
984 inheritance and admixture. Curr. Opin. Immunol. 2014;30C:79–84.

985 14. Mendez FL, Watkins JC, Hammer MF. A Haplotype at STAT2 Introgressed
986 from Neanderthals and Serves as a Candidate of Positive Selection in Papua New
987 Guinea. The American Journal of Human Genetics. Elsevier; 2012;91:265–74.

988 15. Mendez FL, Watkins JC, Hammer MF. Neandertal origin of genetic variation
989 at the cluster of OAS immunity genes. Molecular Biology and Evolution. Oxford
990 University Press; 2013;30:798–801.

991 16. Player MR, Torrence PF. The 2–5 A system: Modulation of viral and cellular
992 processes through acceleration of RNA degradation. Pharmacology &
993 Therapeutics. 1998;78:55–113.

994 17. Mendez FL, Watkins JC, Hammer MF. Global genetic variation at OAS1
995 provides evidence of archaic admixture in Melanesian populations. Molecular
996 Biology and Evolution. 2012;29:1513–20.

997 18. Deschamps M, Laval G, Fagny M, Itan Y, Abel L, Casanova J-L, et al.
998 Genomic Signatures of Selective Pressures and Introgression from Archaic
999 Hominins at Human Innate Immunity Genes. American Journal of Human
1000 Genetics. 2016;98:5–21.

1001 19. Sankararaman S, Mallick S, Patterson N, Reich D. The Combined Landscape
1002 of Denisovan and Neanderthal Ancestry in Present-Day Humans. Current Biology.
1003 2016.

1004 20. Consortium T1GP. A global reference for human genetic variation. Nature.
1005 Nature Publishing Group; 2015;526:68–74.

1006 21. Fu Q, Li H, Moorjani P, Jay F, Slepchenko SM, Bondarev AA, et al. Genome
1007 sequence of a 45,000-year-old modern human from western Siberia. Nature.
1008 2014;514:445–9.

1009 22. Yang MA, Malaspinas AS, Durand EY, Slatkin M. Ancient structure in Africa
1010 unlikely to explain Neanderthal and non-African genetic similarity. Molecular
1011 Biology and Evolution. SMBE; 2012;29:2987–95.

1012 23. Gravel S, Henn BM, Gutenkunst RN, Indap AR, Marth GT, Clark AG, et al.
1013 Demographic history and rare allele sharing among human populations.
1014 Proceedings of the National Academy of Sciences of the United States of America.
1015 National Acad Sciences; 2011;108:11983–8.

1016 24. Tennessen JA, Bigham AW, O'Connor TD, Fu W, Kenny EE, Gravel S, et al.
1017 Evolution and Functional Impact of Rare Coding Variation from Deep Sequencing

of Human Exomes. Science. 2012;337:64–9.

25. Vernot B, Akey JM. Complex History of Admixture between Modern Humans and Neandertals. The American Journal of Human Genetics. 2015.

26. Mathieson I, Lazaridis I, Rohland N, Mallick S, Patterson N, Roodenberg SA, et al. Genome-wide patterns of selection in 230 ancient Eurasians. Nature. 2015.

27. Lazaridis I, Patterson N, Mittnik A, Renaud G, Mallick S, Kirsanow K, et al. Ancient human genomes suggest three ancestral populations for present-day Europeans. Nature. Nature Publishing Group; 2014;513:409–13.

28. Voight BF, Kudaravalli S, Wen X, Pritchard JK. A map of recent positive selection in the human genome. Plos Biology. Public Library of Science; 2006;4:e72.

29. Barreiro LB, Ben-Ali M, Quach H, Laval G, Patin E, Pickrell JK, et al. Evolutionary dynamics of human Toll-like receptors and their different contributions to host defense. Mcvean G, editor. PLoS Genetics. Public Library of Science; 2009;5:e1000562.

30. Sabeti, P.C., Reich DE, Higgins JM, Levine HZP, Richter DJ, Schaffner SF, et al. Detecting recent positive selection in the human genome from haplotype structure. Nature. Nature Publishing Group; 2002;419:832–7.

31. Nauciel C, Espinasse-Maes F. Role of Gamma Interferon and Tumor-Necrosis-Factor-Alpha in Resistance to Salmonella-Typhimurium Infection. Infect. Immun. American Society for Microbiology; 1992;60:450–4.

32. Gulig PA, Doyle TJ, Clare-Salzler MJ, Maiese RL, Matsui H. Systemic infection of mice by wild-type but not Spv- Salmonella typhimurium is enhanced by neutralization of gamma interferon and tumor necrosis factor alpha. Infect. Immun. American Society for Microbiology (ASM); 1997;65:5191–7.

33. LaRock DL, Chaudhary A, Miller SI. Salmonellae interactions with host processes. Nat Rev Micro. 2015;13:191–205.

34. Wu L, Candille SI, Choi Y, Xie D, Jiang L. Variation and genetic control of protein abundance in humans. Nature. 2013;499:79–82.

35. Pickrell JK, Marioni JC, Pai AA, Degner JF. Understanding mechanisms underlying human gene expression variation with RNA sequencing. Nature. 2010;464:768–72.

36. Bonnevie-Nielsen V, Field LL, Lu S, Zheng D-J, Li M, Martensen PM, et al. Variation in antiviral 2',5'-oligoadenylate synthetase (2“5”AS) enzyme activity is controlled by a single-nucleotide polymorphism at a splice-acceptor site in the OAS1 gene. The American Journal of Human Genetics. 2005;76:623–33.

1054 37. Meyer M, Arsuaga JL, de Filippo C, Nagel S, Aximu-Petri A, Nickel B, et al.
1055 Nuclear DNA sequences from the Middle Pleistocene Sima de los Huesos
1056 hominins. Nature. 2016.

1057 38. Lim JK, Lisco A, McDermott DH, Huynh L, Ward JM, Johnson B, et al.
1058 Genetic Variation in OAS1 Is a Risk Factor for Initial Infection with West Nile
1059 Virus in Man. Rice CM, editor. PLoS Pathog. Public Library of Science;
1060 2009;5:e1000321.

1061 39. Bigham AW, Buckingham KJ, Husain S, Emond MJ, Bofferding KM,
1062 Gildersleeve H, et al. Host Genetic Risk Factors for West Nile Virus Infection and
1063 Disease Progression. Ravichandran V, editor. PLoS ONE. Public Library of
1064 Science; 2011;6:e24745.

1065 40. Kwon Y-C, Kang J-I, Hwang SB, Ahn B-Y. The ribonuclease l-dependent
1066 antiviral roles of human 2′,5′-oligoadenylate synthetase family members against
1067 hepatitis C virus. FEBS Letters. 2012;587:156–64.

1068 41. Awady El MK, Anany MA, Esmat G, Zayed N, Tabll AA, Helmy A, et al.
1069 Single nucleotide polymorphism at exon 7 splice acceptor site of OAS1 gene
1070 determines response of hepatitis C virus patients to interferon therapy. Journal of
1071 Gastroenterology and Hepatology. Blackwell Publishing Asia; 2011;26:843–50.

1072 42. Barreiro LB, Quintana-Murci LIS. From evolutionary genetics to human
1073 immunology: how selection shapes host defence genes. Nat Rev Genet. Nature
1074 Publishing Group; 2010;11:17–30.

1075 43. Hancks DC, Hartley MK, Hagan C, Clark NL, Elde NC. Overlapping Patterns
1076 of Rapid Evolution in the Nucleic Acid Sensors cGAS and OAS1 Suggest a
1077 Common Mechanism of Pathogen Antagonism and Escape. Zhang J, editor. PLoS
1078 Genetics. Public Library of Science; 2015;11:e1005203.

1079 44. Kent WJ, Sugnet CW, Furey TS, Roskin KM, Pringle TH, Zahler AM, et al.
1080 The human genome browser at UCSC. Genome Research. Cold Spring Harbor
1081 Lab; 2002;12:996–1006.

1082 45. Hudson R. Generating samples under a Wright–Fisher neutral model of genetic
1083 variation. Bioinformatics. 2002.

1084 46. Chen GK, Marjoram P, Wall JD. Fast and flexible simulation of DNA
1085 sequence data. Genome Research. 2009;19:136–42.

1086 47. Schlamp F, Made J, Stambler R, Chesebrough L, Boyko AR, Messer PW.
1087 Evaluating the performance of selection scans to detect selective sweeps in
1088 domestic dogs. Mol Ecol. 2016;25:342–56.

1089 48. Ferrer-Admetlla A, Liang M, Korneliussen T, Nielsen R. On detecting
1090 incomplete soft or hard selective sweeps using haplotype structure. Molecular

Biology and Evolution. Oxford University Press; 2014;31:1275–91.

49. Huerta-Sanchez E, Jin X, Asan, Bianba Z, Peter BM, Vinckenbosch N, et al. Altitude adaptation in Tibetans caused by introgression of Denisovan-like DNA. Nature. 2014;512:194–7.

50. Excoffier L, Lischer HEL. Arlequin suite ver 3.5: a new series of programs to perform population genetics analyses under Linux and Windows. Molecular Ecology Resources. Blackwell Publishing Ltd; 2010;10:564–7.

51. Maclean CA, Chue Hong NP, Prendergast JGD. hapbin: An Efficient Program for Performing Haplotype-Based Scans for Positive Selection in Large Genomic Datasets. Molecular Biology and Evolution. Oxford University Press; 2015;32:3027–9.

52. Alexander DH, Novembre J, Lange K. Fast model-based estimation of ancestry in unrelated individuals. Genome Research. Cold Spring Harbor Lab; 2009;19:1655–64.

53. Howie BN, Donnelly P, Marchini J. A Flexible and Accurate Genotype Imputation Method for the Next Generation of Genome-Wide Association Studies. Schork NJ, editor. PLoS Genetics. Public Library of Science; 2009;5:e1000529.

54. Storey JD, Tibshirani R. Statistical significance for genomewide studies. Proceedings of the National Academy of Sciences of the United States of America. National Acad Sciences; 2003;100:9440–5.